Chinese Chemical Letters 35 (2024) 109237

Contents lists available at ScienceDirect

Chinese Chemical Letters

journal homepage: www.elsevier.com/locate/cclet

Recent progress of *in situ*/operando characterization techniques for electrocatalytic energy conversion reaction

Zhao Li[a], Huimin Yang[b], Wenjing Cheng[b], Lin Tian[a,b,*]

[a] School of Materials and Chemical Engineering, Xuzhou University of Technology, Xuzhou 221018, China
[b] University and College Key Lab of Natural Product Chemistry and Application in Xinjiang, School of Chemistry and Environmental Science, Yili Normal University, Yining 835000, China

ARTICLE INFO

Article history:
Received 31 May 2023
Revised 18 October 2023
Accepted 23 October 2023
Available online 24 October 2023

Keywords:
In situ techniques
Electrocatalysis
Active sites
Energy conversion

ABSTRACT

Catalysts can significantly promote the reaction dynamics and are therefore considered crucial components for achieving high electrochemical energy conversion efficiency. However, the active sites of the catalysts, particularly for nano-level and atomic-level catalysts commonly undergo reconstruction under practical applications. Therefore, obtaining an in-depth and systematic understanding on the real active sites through *in situ*/operando characterization techniques is a prerequisite for establishing the structure-performance relationship and guiding the future design of more efficient electrocatalysts. Herein, we summarize the recent progress of *in situ*/operando characterization techniques for identifying the nature of active sites of electrocatalysts when used in electrocatalytic energy conversion reaction. Specifically, our focus lies in the fundamental principles of various *in situ*/operando characterization techniques, with particular emphasis on their applications for electrocatalytic reactions. Beyond that, the challenges and perspective insights are also added in the final section to highlight the future direction of this important field.

1. Introduction

The increasing demand in energy for the future development stimulated a great growth in research on pursuing renewable and carbon-neutral energy supplies [1–3]. Nowadays, many efficient conversion technologies, including fuel cells, water splitting, and electrocatalytic CO_2 reduction, play a crucial role and appeal extensive interest as potential approaches to facilitate the energy conversion and supply highly valuable products [4–6]. As well known, catalysts play a crucial role in realizing efficient electrochemical reactions by significantly accelerating reaction kinetics [7–15]. Accordingly, the development of cost-effective and high-performance electrocatalysts is crucial for enhancing the energy conversion process. In essence, the catalysts used for electrochemical reactions should be highly efficient, stable, and economical [16–18]. Despite significant progress in the rational design and fabrication of advanced electrocatalysts, a fundamental question remains unanswered, "what is the nature of active sites under working conditions?" To this end, precisely analyzing the evolution process and comprehensively studying the mechanism are significant for the design and exploration of expected electrocatalysts [19,20].

A deep understanding on the reaction steps, reaction mechanisms, and adsorption energy of intermediates is still lacking, which require more endeavors devoted. In recent years, some advanced *in situ* characterization techniques have been developed to investigate the morphology, structure, composition, and chemical valences of the catalyst [21–23]. Many advanced *in situ* technologies have been well developed for identifying the true reconstruction process of the catalysts, such as the *in situ* Fourier transform infrared spectroscopy [24,25]. Previous works have demonstrated that *in situ* characterization techniques play a pivotal role in deeply understanding the dynamic evolution of reaction sites and the specific reaction mechanisms [26,27]. As expected, *in situ* characterizations have emerged as promising techniques for researchers due to their significant achievements in investigating energy-related reactions [28].

Aiming to describe the recent achievements in this interesting field, we have organized a comprehensive review to summarize the significant advancements *in situ* techniques for studying the reconstruction in the electrochemical reactions (Scheme 1). First, we manifest the fundamental principles of various *in situ* characterization technologies, including XRD, XAS, Raman, FTIR, and TEM. Then, a section on the applications of these *in situ* techniques used

* Corresponding author at: School of Materials and Chemical Engineering, Xuzhou University of Technology, Xuzhou 221018, China.
E-mail address: xzittl@xzit.edu.cn (L. Tian).

https://doi.org/10.1016/j.cclet.2023.109237
1001-8417/

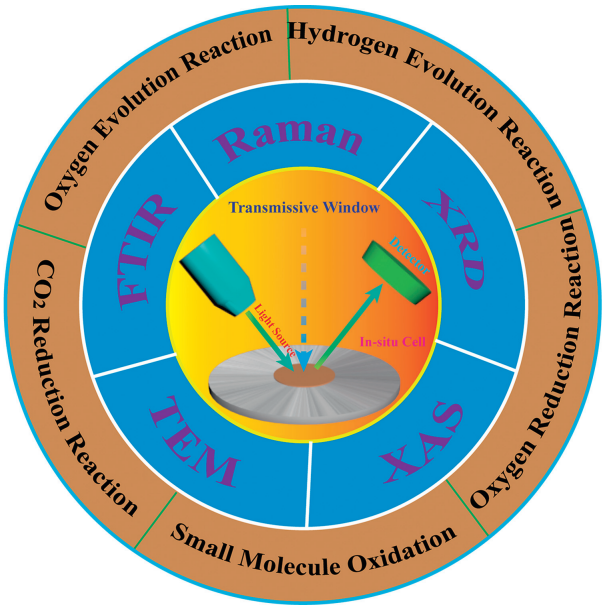

Scheme 1. Scheme of the *in situ* technologies and their applications in energy conversion.

for investigating the dynamic evolution process and the nature of active sites of catalysts during electrochemical operation is also presented. At the end of this review, the future development and application of *in situ* technologies in this fascinating field are systematically discussed.

2. *In situ*/operando characterization techniques

In situ characterization is a technique used to study the properties of materials and surfaces by observing and measuring the structure, morphology, composition and electrochemical properties of materials under *in situ* conditions [29].

The basic principle is to place the material to be studied in an experimental device, and then observe and measure it by various means. These means may include optical microscopy, scanning electron microscopy, transmission electron microscopy, atomic force microscopy, Raman spectrometer, X-ray diffractometer, electrochemical workstation, *etc.* Through these techniques, the changes in structure, morphology, composition and electrochemical properties of materials can be observed and measured in real time [30].

In situ characterization technology has been widely used in materials science, energy storage and conversion, catalyst research, biomedicine and other fields. For example, in the field of materials science, *in situ* characterization technology can be used to study the process of material phase transition, crystal growth, interface reaction, *etc.* In the field of energy-related application, it can be used to study the changes in the performance of energy storage and conversion devices such as batteries and fuel cells. In the research of catalyst, it can be used to study the activity and stability of catalyst. In the biomedical field, it can be used to study properties such as biocompatibility and drug release of biological materials. In short, *in situ* characterization technology provides an important avenue and method for the research of material science and related fields by observing and measuring the property changes of materials under experimental conditions.

2.1. In situ electron microscopy

Electron microscopy, especially for TEM, is one of the most effective strategies for studying the microstructure and morphology

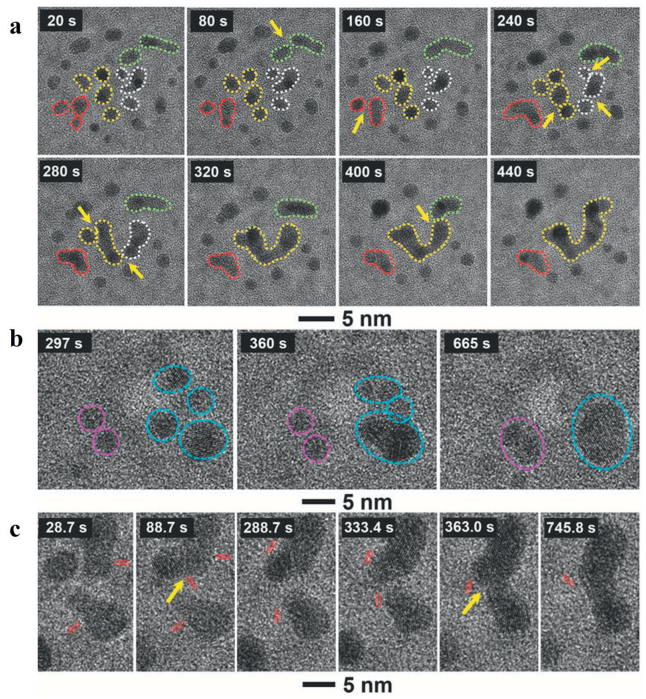

Fig. 1. (a-c) *In situ* TEM observation of Pt nanowire growth at different stages. Reproduced with permission [34]. Copyright 2017, Wiley-VCH.

of the materials [31,32]. The rapid development of TEM analysis techniques has boosted the explosion of nanoscience and nanotechnology. Particularly, *in situ* TEM is now attracting increasing interest as potential characterization technique for revealing the chemical and physical process dynamics at atomic resolutions [33]. For instance, Ma *et al.* [34] demonstrated the syntheses of free-supporting Pt and Pt-Ni nanowire-network electrocatalysts, and the formation mechanism was also investigated by an *in situ* TEM study. According to the *in situ* TEM images (Figs. 1a-c), it was observed that the Pt nanowires were formed through the oriented attachment of individual nanoparticles. Besides *in situ* TEM, a combination of other *in situ* electron microscopy is also demonstrated to be conducive to the investigation of the dynamic structural and morphological evolution during electrocatalysis.

2.2. In situ XRD

XRD shows diffraction patterns for different crystal phases, which can thus be a fingerprint for the analytical task. As well known, the majority of XRD investigations of materials can be used to identify the crystal phases. Therefore, the collection of an XRD pattern can be a potential strategy to study the crystal structures by altering the scattering vector, and XRD is also appearing as a promising technique for analyzing the crystal structure of materials [35] More recently, *in situ* XRD techniques are also developed and used for investigating the crystal plane and structure of the catalysts during electrochemical operation, providing a facile method for monitoring the structure evolution of catalyst and identifying the nature of catalytic active site [36–38]. As an illustration, Yuan *et al.* [39] have studied the structural reconstruction of $Bi(OH)_3$ during electrocatalytic CO_2 reduction reaction (CO_2RR) through a combination of *ex situ* XRD and *in situ* Raman (Figs. 2a-e). Specifically, the sample underwent XRD characterization each 5 mins during the electrochemical activation process in CO_2-saturated 0.1 mol/L $KHCO_3$ at -1.0 V_{RHE}. According to the *ex situ* XRD pattern, it is clearly observed that the peaks at 47.0°, 42.4°, and 32.9° can be indexed to the $Bi(OH)_3$, while the

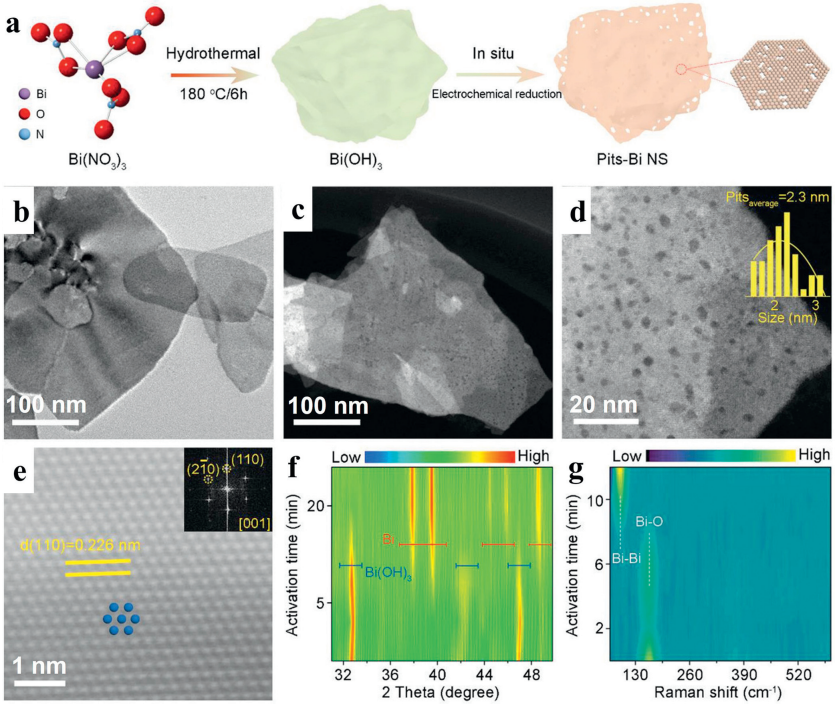

Fig. 2. (a) Illustration of the fabrication of $Bi(OH)_3$ and the reconstruction to pits-Bi nanosheets. (b) TEM image, (c, d) STEM image and (e) AC-STEM image of the pits-Bi nanosheets. (f) *Ex situ* XRD and (g) Raman spectra for the *in situ* reconstruction process. Reproduced with permission [39]. Copyright 2022, Wiley-VCH.

other peak located at 48.7°, 45.9°, 44.6°, 39.6° and 37.9° are associated with the metallic Bi (Figs. 2f and g). The *ex situ* XRD pattern suggested that the transformation of $Bi(OH)_3$ to metallic Bi during electrocatalytic CO_2RR.

2.3. In situ Raman

The principle of *in situ* Raman spectroscopy is to use the scattering phenomenon that the incident light frequency is obviously changed by material surface molecules [40–43]. Operando Raman spectroscopy is also conducted to establish the evolution of electrocatalysts during reactions process and emerging as a potential approach to explore the structure-performance relationship of catalysts. For example, Wu *et al.* [44] have performed the *in situ* surface-enhanced Raman analysis to clarify the role of cation defect of the catalyst during electrochemical reaction. Specifically, they have synthesized the defective NiFe-LDH nanosheets *via* a facile aprotic-solvent-solvation-induced strategy. According to the Raman spectra, it is clearly observed that the as-generated cationic vacancy defects tend to exist as V_M (M = Ni/Fe) (Figs. 3a and b). As the voltage increases, the crystalline $Ni(OH)_x$ on the surface of NiFe-LDH gradually transforms into a disordered state. When oxygen bubbles begin to evolve under sufficiently high voltage, local NiOOH species appear as residual products (Figs. 3c and d). Therefore, *in situ* Raman spectra are beneficial for understanding the reconstruction behaviors of the NiFe-LDH. Besides better understanding the surface reconstruction process, *in situ* Raman technology is also advantageous for providing insights into the adsorption and transfer of the reaction intermediates. Previous studies have reported that *in situ* Raman technology can be utilized to identify the electron transfer and hydrogen spillover effects, which are critical for comprehending the reaction mechanisms.

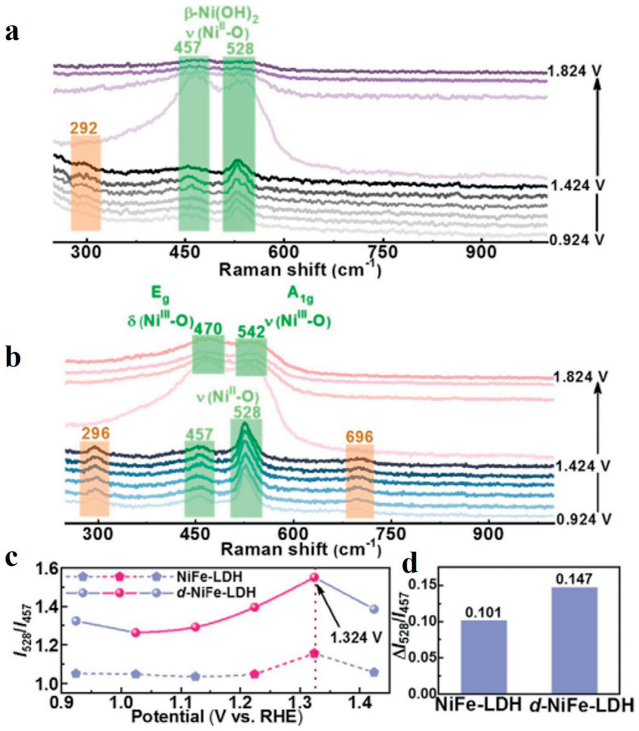

Fig. 3. *In situ* Raman spectroscopy tests for studying the transformation of (a) the pristine NiFe-LDH and (b) D-NiFe-LDH during OER. (c, d) The evolution of I_{528}/I_{457} of NiFe-LDH and D-NiFe-LDH. Reproduced with permission [44]. Copyright 2021, Wiley-VCH.

2.4. In situ FTIR

In situ FTIR, pioneered by Bewick *et al.* [24] has been utilized to acquire the molecular information regarding ionic and neutral adsorbates at the electrode as well as solution species during electrochemical reactions [45,46]. *In situ* FTIR is employed to characterize the adsorbates, molecules, and the intermediated species. Many researches employed *in situ* FTIR to study the electrocatalytic pro-

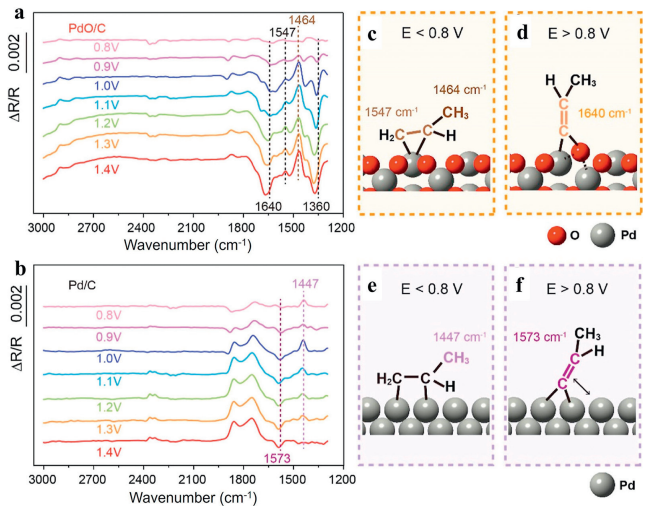

Fig. 4. *In situ* ATR-FTIR spectra of C_3H_6 oxidation on (a) PdO/C and (b) Pd/C at different potentials in a C_3H_6-saturated 0.1 mol/L $HClO_4$ solution. Different propene adsorbed configurations (c) on PdO below 0.80 V, (d) above 0.8 V, (e) on Pd below 0.80 V, and (f) above 0.80 V. Reproduced with permission [50]. Copyright 2021, American Chemical Society.

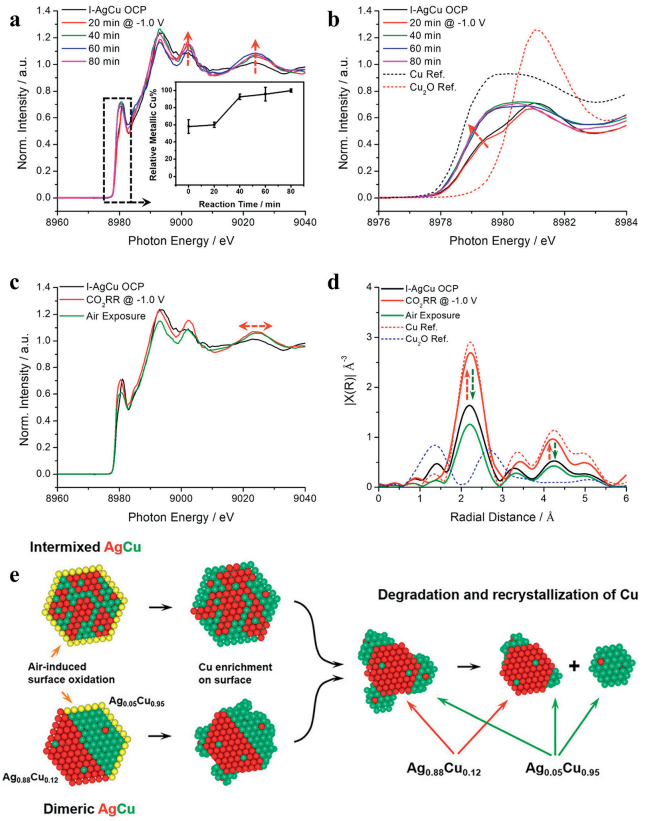

Fig. 5. (a) Operando XANES of Cu K-edge of the I-AgCu as a function of the reaction time at −1.0 V *vs.* RHE in CO_2-saturated 0.1 mol/L $KHCO_3$. (b) XANES pre-edges of I-AgCu magnified from the dashed box region in (a) and the comparison with Cu and Cu_2O references (dashed lines). (c, d) Operando XANES and EXAFS spectra of I-AgCu for CO_2RR. (e) The *in situ* evolution of intermixed and phase-separated AgCu catalysts in electrochemical CO_2RR. Reproduced with permission [58]. Copyright 2023, American Chemical Society.

cesses, including the study of the reaction mechanisms of organic molecules oxidation, CO_2RR, and the corresponding dynamic process [47,48]. Sun *et al.* have used this technique to investigate the reaction mechanism and intermediated species of many electrocatalytic processes [49]. For instance, they have investigated the reaction mechanisms of the propene electrooxidation on Pd/C and PdO/C *via in situ* FTIR [50]. Based on the *in situ* attenuated total reflection FTIR (Figs. 4a and b), a novel reaction pathway was distinctly observed compared with unconventional thermocatalysis (Figs. 4c-f). This work highlights the significant role of *in situ* FTIR in elucidating the electrochemical reaction mechanisms involved in propene oxidation.

2.5. Operando XAS

XAS is extensively employed to investigate the local electronic and atomic structure of catalysts [51–53]. Compared with the XRD, XAS is sensitive to the electronic structure of materials, which can thus be utilized as advanced characterizations to measure the electronic properties of the catalysts [54]. Recently, XAS characterization techniques have been widely utilized in the electronic structure analysis of nanocatalysts and single-atom catalysts [55], which have gained widespread utilization and extensive investigation [56,57]. For example, Yang and coworkers explored the structural and chemical transformation of the AgCu nanocatalysts during the electrochemical CO_2RR [58]. According to a systematic investigation, it has been revealed that the two types of catalysts undergo similar structural evolution under CO_2RR conditions (Figs. 5a-d). In the case of intermixed AgCu catalysts, Cu may undergo leaching and subsequently become enriched on the surface of particles or recrystallize elsewhere as new particles (Fig. 5e).

3. Applications of *in situ*/operando characterization techniques for electrocatalytic reactions

3.1. ORR

Fuel cells offer a green and high-efficiency technology for the conversion of chemical energy into electrical energy [59,60]. The development of high-performance ORR catalysts largely relies on a comprehensive understanding on the redox behavior of the active sites [61–67]. Therefore, the *in situ*/operando measurement techniques are highly imperative [68–71]. Recent works have confirmed the significant role of *in situ* techniques in enhancing our understanding on the redox behavior of metal sites during electrochemical ORR. For instance, Huang and colleagues reported the *in situ* synthesis of Ru-doped Pt_3Co octahedral nanoparticles grown on carbon (Ru–Pt_3Co/C) [72], which exhibited remarkable ORR activity up to 1.05 A/mg_{Pt}. Ru doping effectively mitigates Co corrosion, substantially improving the morphological stability of Ru-Pt_3Co/C. *In situ* XAFS analysis revealed that Ru promoted the Pt atom inversion (Figs. 6a-d), thereby limiting over-reduction of Pt sites to enhance the stability of Ru-Pt_3Co/C. Additionally, DFT calculations demonstrated that adding Ru atom accelerated the oxygen intermediate breach and desorption (Fig. 6e).

In situ characterization techniques can be employed not only to investigate the nature of active sites, but also to examine the intermediates during electrochemical ORR [73]. Dong *et al.* employed the shell-isolated nanoparticle-enhanced Raman spectroscopy (SHINERS) to study the ORR mechanism at Pt (211) and Pt (311) surfaces [74]. Through control and isotope substitution experiments, clear evidence of OH and OOH intermediates at Pt (311) and Pt (211) surfaces can be observed. It was concluded that the difference in OOH adsorption on high-index surfaces posed a significant impact on the electrocatalytic ORR performance (Figs. 6f and g). The research has enhanced the comprehension of ORR mechanism on high-index Pt (*hkl*) surface and highlighted the crucial significance of *in situ* techniques for a thorough understanding of the ORR mechanism.

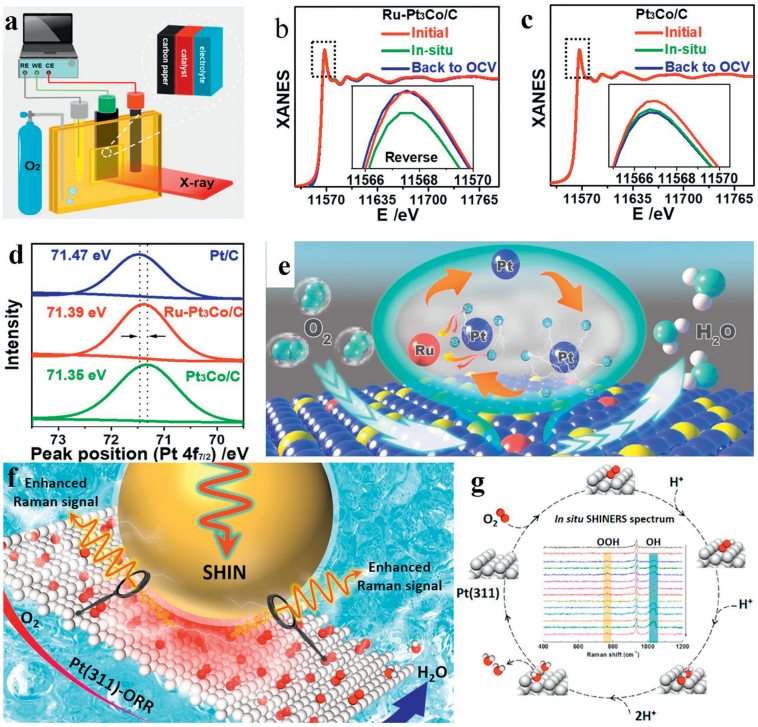

Fig. 6. *In situ* XAS tests. (a) Scheme of the electrochemical setup for the *in situ* XAS experiment. Pt L_3-edge XANES spectra of (b) Ru-Pt_3Co/C and (c) Pt_3Co/C during the ORR. (d) Peak positions of Pt $4f_{7/2}$ XPS spectra for Ru-Pt_3Co/C, Pt_3Co/C, and commercial Pt/C. (e) The corresponding ORR mechanism of Ru-Pt_3Co/C. Schematic illustration of the (f) SHINERS study of the ORR at Pt (311) surface and the (g) ORR mechanism. (a-e) Reproduced with permission [72]. Copyright 2021, American Chemical Society. (f, g) Reproduced with permission [74]. Copyright 2020, American Chemical Society.

3.2. Small molecule oxidation

The electrooxidation of hydrogen, CO, or small organic molecules is also a crucial electrode reaction of fuel cells [75,76]. Appraising the reaction intermediates is of crucial importance to unveil the pathways and mechanisms. Taking electrocatalytic hydrogen oxidation reaction (HOR) as an example, the HOR may follow the Heyrovsky-Volmer or Tafel-Volmer mechanism in acidic solution, where the H^+ can be generated on the catalyst surface from adsorbed hydrogen and then convert to a proton by releasing an electron [77,78]. The EOR process typically involves a dual-pathway mechanism, namely the C1 and C2 pathways. The former can generate adsorbed carbon monoxide (CO_{ad}) and carbonate radical (CO_3^{2-}) intermediates [79–82]. In contrast, the C2 pathway is involved in the generation of acetate radical (CH_3COO^-). Therefore, measuring and analyzing the intermediated species will be significant for deeply understanding on the reaction pathways and mechanisms. Huang and coworkers investigated the EOR mechanism on the Pd-Sb hexagonal nanoplate (Figs. 7a-d) [83]. According to the *in situ* ATR-SEIRAS spectra, it is clearly found that there are two forms of CO adsorption on Pd_8Sb_3 HPs/C surface (bridge-bonded CO (CO_B) and multiply-bonded CO (CO_M)), while Pd/C has three forms of CO adsorption (linear-bonded CO (CO_L), CO_B and CO_M) (Figs. 7e and f). The negligible CO_L on Pd_8Sb_3 HPs/C reveals that the linear CO adsorption capacity of Pd_8Sb_3 HPs/C is weakened due to the introduction of Sb, and the stronger CO_M and CO_B on Pd_8Sb_3 HPs/C suggest a more positive CO, indicating that Pd_8Sb_3 HPs/C can greatly facilitate the C_2 pathway of the EOR.

Guo *et al.* employed the *in situ* FTIR test to obtain in-depth understanding on the improvement MOF performance on the YO_x/MoO_x-Pt catalyst (Figs. 7g-i) [84]. *In situ* FTIR spectra showed several bands between 2500 cm^{-1} and 1000 cm^{-1}, where the downward bands at 2341 cm^{-1} was assigned to the asymmetric stretching vibration of CO_2, implying the complete oxidation of methanol (Figs. 7j-m). It was also demonstrated that MoO_x and YO_x contributed to the enhanced anti-CO poisoning capability of Pt nanowires. Moreover, DFT calculations further revealed that surface Y and Mo atoms, with enabled oxidation states, facilitated the binding of COOH* to the surface *via* both C and O atoms. This effectively reduced the free energy barriers for CO* oxidation into COOH*. As a result, a mass activity of 2.10 A/mg_{Pt} and a high specific activity of 3.35 mA/cm^2 were achieved for the optimized 22% YO_x/MoO_x-Pt.

3.3. OER

OER plays a critical role in electrochemical water splitting as it involves a four-electron transfer process, which directly determines the energy barrier and reaction efficiency of the overall reaction [85–90]. Therefore, significant efforts have been dedicated to the development and production of more efficient electrocatalysts to enhance the reaction kinetics of OER [90–92]. It is demonstrated that the *in situ* characterizations play a key role in identifying the nature of true active sites of catalysts during OER [93–95]. For instance, Zheng *et al.* [96] endeavored to explore the electrochemical reconstruction of MOFs and elucidate the function of *in situ* generated species during electrochemical OER (Figs. 8a and b). Dramatic morphological changes that expose electron-accessible Co sites are clearly observed (Figs. 8c-e). Subsequent OER experiments suggest that the dominating active sites are CoOOH species produced from α/β-$Co(OH)_2$.

3.4. HER

Electrocatalytic HER offers a promising strategy to provide clean energy carriers to alleviate the energy crisis [97–101]. According to the Sabatier's principle and volcano plot of hydrogen intermediate

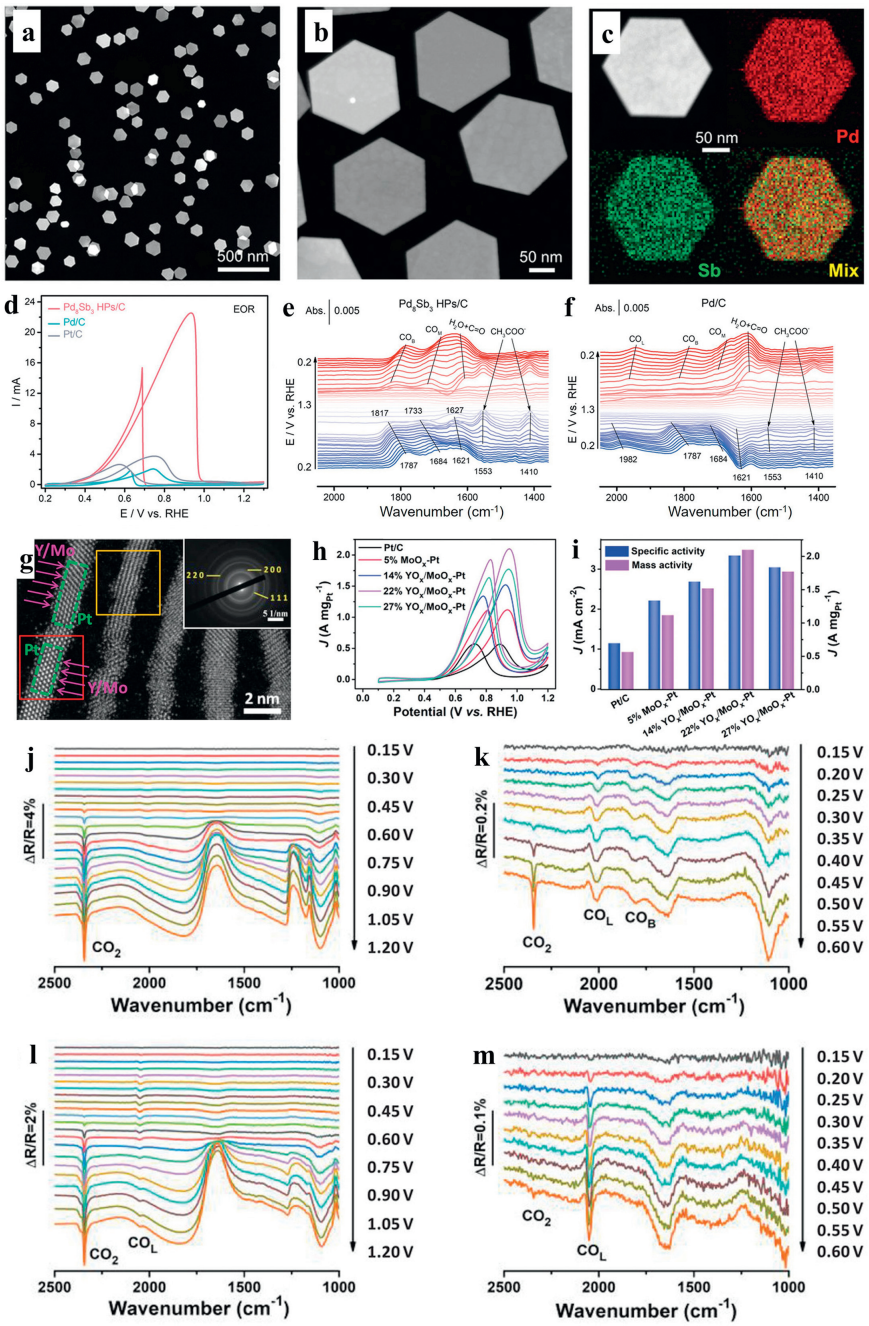

Fig. 7. (a, b) HAADF-STEM images and the (c) elemental mapping images of the Pd_8Sb_3 HPs. (d) CV curves of the Pd_8Sb_3 HPs/C, Pd/C, and Pt/C for EOR. *In situ* ATR-SEIRAS spectra of (e) Pd_8Sb_3 HPs/C and (f) Pd/C during CV cycling. (g) Atomic-resolution HAADF-STEM image of the 22% YO_x/MoO_x-Pt nanowires. (h) Pt mass-normalized MOR, (i) comparison on the specific activities and mass activities of 22% YO_x/MoO_x-Pt nanowires and other references. (j) *In situ* FTIR spectra recorded from 0.15 V to 1.20 V and (k) magnified *in situ* FTIR spectra recorded from 0.15 V to 0.60 V *versus* RHE during MOR on 22% YO_x/MoO_x-Pt. (l, m) *In situ* FTIR spectra during MOR. (a-f) Reproduced with permission [83]. Copyright 2022, Wiley-VCH. (g-m) Reproduced with permission [84]. Copyright 2021, Wiley-VCH.

adsorption (ΔG_H), the best HER catalyst should possess the close-to-zero ΔG_H [102,103]. To this end, designing the synthesizing the advanced HER electrocatalysts with close-to-zero ΔG_H is highly favorable for promoting the hydrogen production [104]. However, it is also demonstrated that the hydrogen spillover effect and surface reconstruction of catalyst during electrochemical reactions are also crucial for affecting the HER performance [105–108]. Operating *in situ* characterization tests is imperative to understand the reaction mechanisms and reconstruction process of catalyst, which will provide guidance for future rational design and fabrication of more excellent HER catalysts. Using Wei's work as an example, they have reported the preparation of Pt/TiO_2 catalyst with abundant deficient oxygen vacancies (V_O-deficient Pt/TiO_2) and rich oxygen vacancies (V_O-rich Pt/TiO_2) (Figs. 9a-c) [109]. Remarkably, it is measured that the V_O-rich Pt/TiO_2 has a mass activity of 45.28 A/mg_{Pt} at −0.1 V *vs.* RHE, which is 58.8 and 16.7 times higher than those of commercial Pt/C and V_O-deficient Pt/TiO_2, respectively (Figs. 9d and e). In order to uncover the outstanding electrocatalytic HER performance, they have operated the *in situ* Raman tests and DFT calculations. Based on the *in situ* Raman spectra, it is obviously observed the H^* transfer from Pt to TiO_2 support. In contrast, no obvious peak related with $E_{g(1)}$ are observed during the catalytic process due to the absence of H^* (Fig. 9f). DFT calculations have demonstrated that TiO_2 with abundant oxygen vacancies can facil-

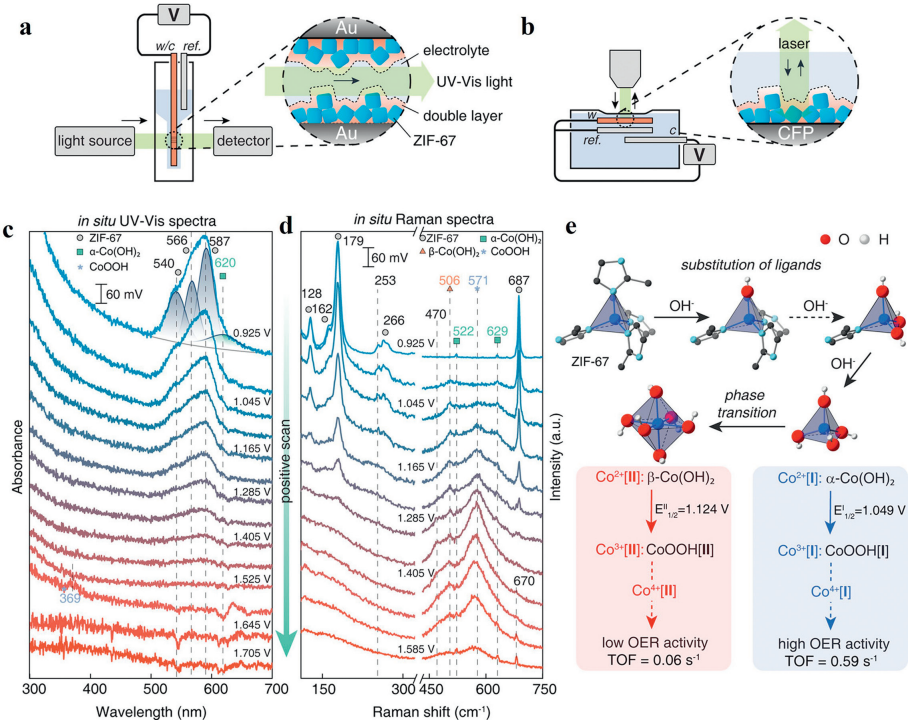

Fig. 8. (a) *In situ* UV–vis and (b) Raman devices. (c) *In situ* UV–vis spectroelectrochemical study between 0.925 V and 1.705 V. (d) *In situ* Raman spectroelectrochemical study between 0.925 V and 1.585 V. (e) Scheme for the transformation of ZIF-67 to α-$Co(OH)_2$ and β-$Co(OH)_2$. Reproduced with permission [96]. Copyright 2019, American Chemical Society.

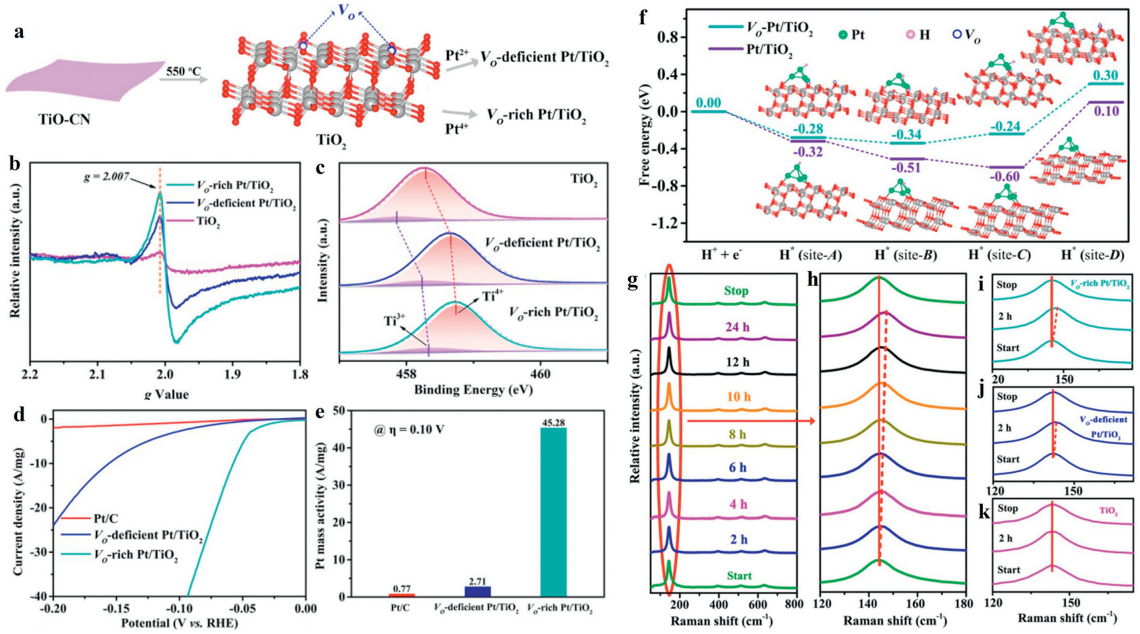

Fig. 9. (a) Illustration of the synthesis procedures of the V_O-rich Pt/TiO_2 and V_O-deficient Pt/TiO_2 catalysts. (b) ESR spectra and (c) XPS profiles. (d) HER polarization curves and (e) corresponding mass activity at the overpotential of 100 mV. (f) DFT calculation of the free energy. (g) *In situ* Raman spectra of V_O-rich Pt/TiO_2 at −0.1 V *vs.* RHE with different electrolysis durations. (h) Magnified view of the $E_{g(1)}$ mode. (i–k) *In situ* Raman spectra of V_O-rich Pt/TiO_2 (i), V_O-deficient Pt/TiO_2 (j), and TiO_2 (k) at a potential of −0.2 V *vs.* RHE. Reproduced with permission [109]. Copyright 2021, Wiley-VCH.

itate both reversed charge transfer and hydrogen spillover from Pt to the TiO_2 support, thereby contributing to the improved electrocatalytic performance for HER (Figs. 9g-k).

3.5. CO_2RR

Electrocatalytic CO_2RR is a promising renewable technology for the conversion of greenhouse gas into value-added liquid fuels and chemicals [110,111]. Cu, Pd, Pb, and Bi-based catalysts are established as the predominant candidate for selective CO_2 electroreduction to multicarbon products [111–113]. However, the comprehension of the nature of active sites during reaction conditions remains limited, particularly for some electrocatalysts with complicated components. To this end, *in situ* characterization technologies are emerging as promising candidates for addressing these issues. Yang and colleagues emphasized the importance of under-

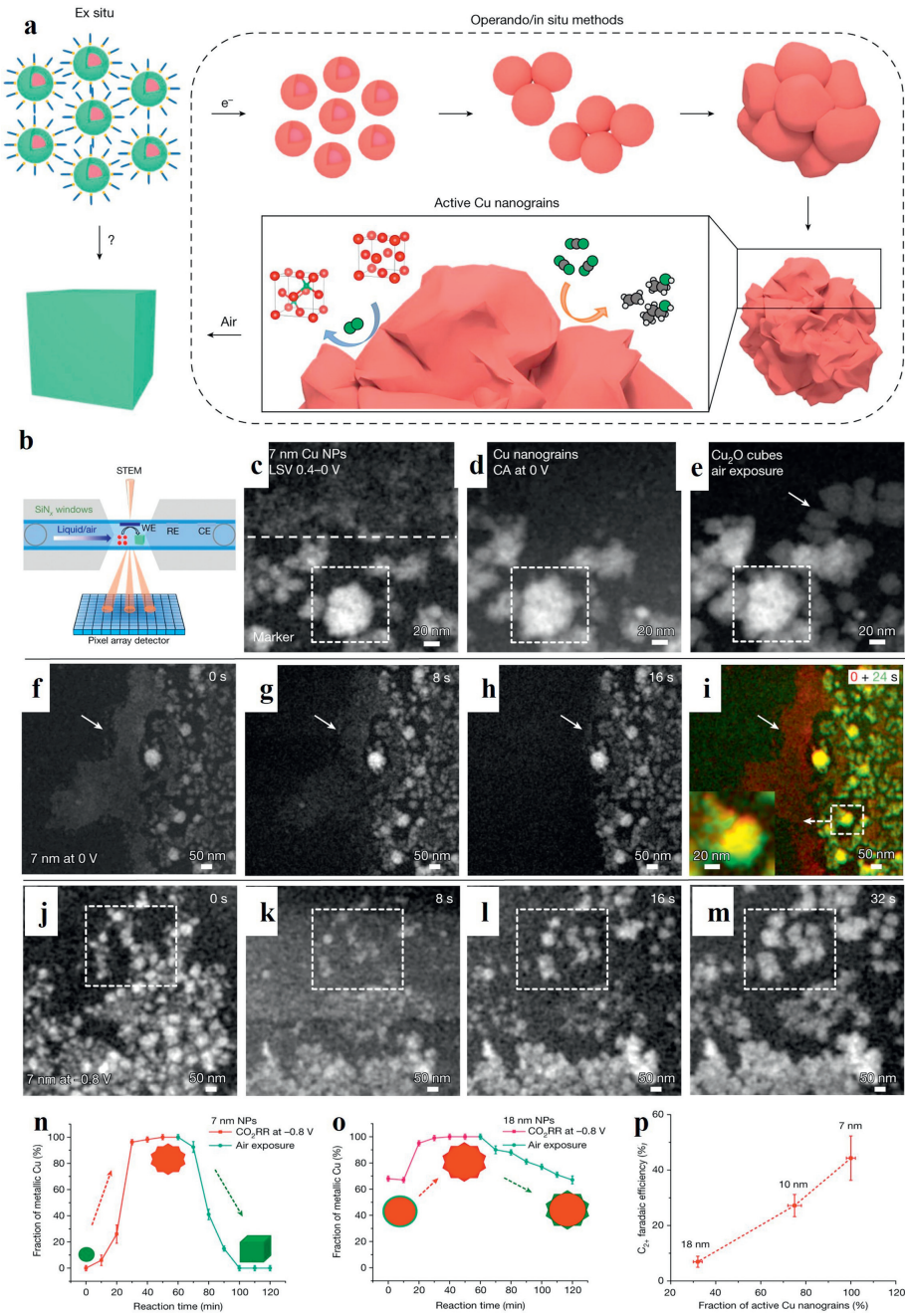

Fig. 10. (a) Operando/*in situ* methods used to reveal the dynamic changes during electrocatalytic CO_2RR. (b) Scheme of operando EC-STEM and 4D-STEM under CO_2RR-relevant conditions. (c-m) EC-STEM images of the initial growth of Cu nanocatalysts after a single negative-direction LSV scan, from 0.4 V to 0 V. (n) Quantitative analysis of relative fraction of metallic Cu. Operando XANES (o) and corresponding quantitative analysis (p) of 18 nm nanoparticles at −0.8 V. Reproduced with permission [115]. Copyright 2023, Nature Publishing Group.

standing and regulating the dynamic characteristics of nanocatalysts to attain optimized CO_2 electrolysis [114]. Specifically, they have systematically investigated the dynamic aspects of both the active site and its surrounding reaction microenvironment by analyzing the structural transformation *via in situ*/operando characterizations [115]. More recently, they also identified the nature of reaction sites of the high-activity Cu nanocatalysts through time-resolved operando techniques (Figs. 10a and b). After a systematic investigation, it is clearly found that an ensemble of monodisperse Cu nanoparticles would undergo a structural transformation process. According to the operando EC-STEM image, 4D-STEM image and XANES spectra, it is uncovered that the Cu nanograins underwent a typical structural reconstruction (Figs. 10c-m). As a result, a 7 nm Cu nanoparticle ensemble, with a unity fraction of active Cu nanograins, exhibits sixfold higher C_{2+} selectivity than the 18 nm counterpart with one-third of active Cu nanograins (Figs. 10n-p).

4. Conclusion and perspectives

In summary, we have focused on the *in situ* characterizations utilized for identifying the true active sites of catalyst and better understanding the reaction mechanism of electrocatalytic reactions. The aim of this review is to clarify the great significance of the *in situ* characterization techniques on various electrocatalytic reactions. By systematically discussing the fundamentals of various *in situ* technologies, such as *in situ* electron microscopy, *in situ*

XRD, *in situ* FTIR, *in situ* Raman, *in situ* XAS, we hope to provide readers with insightful ideas about the development of *in situ* technologies. Subsequently, the applications of various *in situ* technologies used for identifying the nature of reaction sites and the surface adsorption of intermediated species are also discussed in detail, which will benefit for the development of advanced electrocatalysts. Despite the significant progress achieved in this interesting field, a comprehensive visualization is still far from being attained. More efforts need to be devoted and some challenges must also be overcome.

Notably, many factors can govern the electrocatalytic performance of the catalysts, including the oxidation state, local electronic structure. Refining the monitoring of electrocatalytic processes through a single *in situ* technique and interpretation of mechanisms may result in an incomplete assessment. Therefore, it is of utmost importance to integrate multiple *in situ* analytical techniques to provide a comprehensive insight into the underlying mechanisms of electrochemical reactions.

In addition, it should be noted that a significant disparity exists between the *in situ* employed devices and actual energy devices. Currently, most researches are focused on the half-reaction of energy conversion devices, such as detecting the intermediates of small molecules in fuel cells. To this end, optimizing the electrochemical performance of *in situ* cells related to real energy devices should be the future direction.

Another important challenge that should be overcome is to establish a reconstruction-performance relationship. Previous works have demonstrated that the *in situ* reconstruction of some catalysts can yield highly active species to further enhance the electrocatalytic performance, while some are hindering the surface reconstruction to achieve high electrocatalytic performance. For example, the surface reconstruction of $Ni(OH)_2$ can yield highly active NiOOH to boost electrocatalytic OER, while some works are hampering the surface reconstruction of $Ni(OH)_2$ by incorporating the Fe^{3+}. It is still unclear whether surface reconstruction can promote the electrocatalytic performance or not.

Declaration of competing interest

The authors declare that they have no known competing financial interests or personal relationships that could have appeared to influence the work reported in this paper.

Acknowledgments

This work was financed by the National Natural Science Foundation of China (No. 22202169), Xuzhou Science and Technology Plan Project of China (No. KC21294).

References

[1] Y. Yue, P. Cai, K. Xu, et al., J. Am. Chem. Soc. 143 (2021) 18052–18060.
[2] Y.R. Hong, S. Dutta, S.W. Jang, et al., J. Am. Chem. Soc. 144 (2022) 9033–9043.
[3] J. Qin, H. Liu, P. Zou, et al., J. Am. Chem. Soc. 144 (2022) 2197–2207.
[4] H.Q. Fu, M. Zhou, P.F. Liu, et al., J. Am. Chem. Soc. 144 (2022) 6028–6039.
[5] J. Yang, H. Qi, A. Li, et al., J. Am. Chem. Soc. 144 (2022) 12062–12071.
[6] J. Liu, W. Niu, G. Liu, et al., J. Am. Chem. Soc. 143 (2021) 4387–4396.
[7] L. Zhang, J. Liang, L. Yue, et al., Nano Res. Energy 1 (2022) 9120028.
[8] L. Zhang, L. Li, J. Liang, et al., Inorg. Chem. Front. 10 (2023) 2766–2775.
[9] T. Xu, D. Ma, T. Li, et al., Chem. Commun. 56 (2020) 14031–14034.
[10] L. Ouyang, X. He, Y. Sun, et al., Inorg. Chem. Front. 9 (2022) 6602–6607.
[11] L. Tian, Y. Liu, C. He, et al., Chem. Rec. 23 (2023) e202200213.
[12] L. Tian, Z. Huang, X. Lu, et al., Inorg. Chem. 62 (2023) 1659–1666.
[13] X. Lu, T. Wang, M. Cao, et al., Int. J. Hydrogen Energy 48 (2023) 34740–34749.
[14] X. Lu, M. Du, T. Wang, et al., Int. J. Hydrogen Energy 48 (2023) 34009–34017.
[15] L. Tian, X. Pang, H. Xu, et al., Inorg. Chem. 61 (2022) 16944–16951.
[16] H. Xu, L. Yang, K. Wang, et al., Inorg. Chem. 62 (2023) 11271–11277.
[17] H. Xu, K. Wang, L. Jin, et al., J. Colloid Interface Sci. 650 (2023) 1500–1508.
[18] H. Xu, K. Wang, G. He, et al., J. Mater. Chem. A 11 (2023) 17609–17615.
[19] P. Geng, L. Wang, M. Du, et al., Adv. Mater. 34 (2022) e2107836.
[20] M. Du, P. Geng, C. Pei, et al., Angew. Chem. Int. Ed. 61 (2022) e202209350.
[21] D. Friebel, V. Viswanathan, D.J. Miller, et al., J. Am. Chem. Soc. 134 (2012) 9664–9671.
[22] L. Huang, J.Y. Sun, S.H. Cao, et al., ACS Catal. 6 (2016) 7686–7695.
[23] Z. Zhao, Z. Yuan, Z. Fang, et al., Adv. Sci. 5 (2018) e1800760.
[24] J.Y. Ye, Y.X. Jiang, T. Sheng, et al., Nano Energy 29 (2016) 414–427.
[25] X. Hu, Z. Xiao, W. Wang, et al., J. Am. Chem. Soc. 145 (2023) 15109–15117.
[26] X. Chen, W. Li, G. Zhang, et al., Mater. Today Chem. 23 (2022) 100705.
[27] H. Zhou, S. Zheng, X. Guo, et al., J. Colloid Interface Sci. 628 (2022) 24–32.
[28] Y. Wang, Y. Li, T. Heine, J. Am. Chem. Soc. 140 (2018) 12732–12735.
[29] J. Liu, L. Guo, Matter 4 (2021) 2850–2873.
[30] J. Zhao, J. Lian, Z. Zhao, Nano Micro Lett. 15 (2022) 19.
[31] S. Liu, Y. Zhang, X. Mao, Energy Environ. Sci. 15 (2022) 1672–1681.
[32] M. Wang, M. Wang, C. Zhan, et al., J. Mater. Chem. A 10 (2022) 18972–18977.
[33] C. Zhang, K.L. Firestein, J.F.S. Fernando, et al., Adv. Mater. 32 (2020) e1904094.
[34] Y. Ma, W. Gao, H. Shan, et al., Adv. Mater. 29 (2017) e1703460.
[35] S. Tang, Y. Zhou, X. Lu, et al., J. Alloys Compds. 924 (2022) 166415.
[36] S. Liu, H. Ji, M. Wang, et al., ACS Appl. Mater. Interfaces 12 (2020) 15298–15304.
[37] Y. Qiu, L. Xin, Y. Li, et al., J. Am. Chem. Soc. 140 (2018) 16580–16588.
[38] Z. Yan, H. Sun, X. Chen, et al., Nat. Commun. 9 (2018) 2373.
[39] Y. Yuan, Q. Wang, Y. Qiao, et al., Adv. Energy Mater. 12 (2022) e202200970.
[40] S.K. Geng, Y. Zheng, S.Q. Li, et al., Nat. Energy 6 (2021) 904–912.
[41] Y. Bai, Y. Wu, X. Zhou, et al., Nat. Commun. 13 (2022) 6094.
[42] S.S. Mishra, P. Kumbhakar, S. Nellaiappan, et al., Energy Technol. 11 (2022) e202200860.
[43] X. Zhang, H. Yi, M. Jin, et al., Small 18 (2022) e2203710.
[44] Y.J. Wu, J. Yang, T.X. Tu, et al., Angew. Chem. Int. Ed. 60 (2021) 26829–26836.
[45] Y. Wang, M. Zheng, Y. Li, et al., Angew. Chem. Int. Ed. 61 (2022) e202115735.
[46] Y. Wang, M. Zheng, H. Sun, et al., Appl. Catal. B: Environ. 253 (2019) 11–20.
[47] Z.Y. Wu, Y.Q. Lu, J.T. Li, et al., ACS Omega 6 (2021) 27335–27350.
[48] J.X. Tang, L.P. Xiao, C. Xiao, et al., J. Mater. Chem. A 9 (2021) 11049–11055.
[49] J.X. Tang, N. Tian, L.P. Xiao, et al., J. Mater. Chem. A 10 (2022) 10902–10908.
[50] X.C. Liu, T. Wang, Z.M. Zhang, et al., J. Am. Chem. Soc. 144 (2022) 20895–20902.
[51] S. Liu, H. Zhang, H. Yu, et al., Small 19 (2023) e2300388.
[52] E. Marelli, J. Gazquez, E. Poghosyan, et al., Angew. Chem. Int. Ed. 60 (2021) 14609–14619.
[53] J. Wang, C. Cheng, B. Huang, et al., Nano Lett. 21 (2021) 980–987.
[54] Q. Wang, X. Huang, Z.L. Zhao, et al., J. Am. Chem. Soc. 142 (2020) 7425–7433.
[55] M. Xie, S. Tang, B. Zhang, et al., Mater. Horiz. 10 (2023) 407–431.
[56] Y. Zhu, T.R. Kuo, Y.H. Li, et al., Energy Environ. Sci. 14 (2021) 1928–1958.
[57] M. Wang, L. Arnadottir, Z.J. Xu, et al., Nano Micro Lett. 11 (2019) 47.
[58] P.C. Chen, C. Chen, Y. Yang, et al., J. Am. Chem. Soc. 145 (2023) 10116–10125.
[59] X. Chu, J. Li, W. Qian, et al., Chem. Rec. 23 (2023) e202200222.
[60] X. Chu, L. Wang, J. Li, et al., Chem. Rec. 23 (2023) e202300013.
[61] Z. Wang, S. Xu, M. Li, et al., Chem. Commun. 59 (2023) 4511–4514.
[62] Y. Sheng, Y. Guo, H. Yu, et al., Small 19 (2023) e2207305.
[63] C. Xu, C. Guo, J. Liu, et al., Small 19 (2023) e2207675.
[64] Y. He, Y. Jia, B. Yu, et al., Small 19 (2023) e2206478.
[65] L. Li, N. Li, J. Xia, et al., J. Mater. Chem. A 11 (2023) 2291–2301.
[66] L. Li, N. Li, J.W. Xia, et al., Nano Res 16 (2023) 9416–9425.
[67] D. Deng, S. Wu, H. Li, et al., Small 19 (2023) e2205469.
[68] H. Lu, Y. Jiang, G. Xiao, et al., J. Colloid Interface Sci. 616 (2022) 539–547.
[69] L. Tao, M. Sun, Y. Zhou, et al., J. Am. Chem. Soc. 144 (2022) 10582–10590.
[70] W. Deeloed, T. Priamushko, J. Cizek, et al., ACS Appl. Mater. Interfaces 14 (2022) 23307–23321.
[71] S. Kim, S. Ji, H. Yang, et al., Appl. Catal. B: Environ. 310 (2022) 121361.
[72] Y. Zhu, J. Peng, X. Zhu, et al., Nano Lett. 21 (2021) 6625–6632.
[73] L. Cao, X. Liu, X. Shen, et al., Acc. Chem. Res. 55 (2022) 2594–2603.
[74] J.C. Dong, M. Su, V. Briega-Martos, et al., J. Am. Chem. Soc. 142 (2020) 715–719.
[75] H. Xu, B. Huang, Y. Zhao, et al., Inorg. Chem. 61 (2022) 4533–4540.
[76] X. Chu, K. Wang, W. Qian, et al., Coord. Chem. Rev. 477 (2023) 214952.
[77] C. Zhan, L. Bu, H. Sun, et al., Angew. Chem. Int. Ed. 62 (2023) e202213783.
[78] V.H. Do, P. Prabhu, V. Jose, et al., Adv. Mater. 35 (2023) e2208860.
[79] M. Zhou, J. Liu, C. Ling, et al., Adv. Mater. 34 (2022) e2106115.
[80] C. Liu, Y. Shen, J. Zhang, et al., Adv. Energy Mater. 12 (2022) e202103505.
[81] W. Chen, S. Luo, M. Sun, et al., Adv. Mater. 34 (2022) e2206276.
[82] G. Liu, W. Zhou, Y. Ji, et al., J. Am. Chem. Soc. 143 (2021) 11262–11270.
[83] Y. Zhang, X. Liu, T. Liu, et al., Adv. Mater. 34 (2022) e2202333.
[84] M. Li, Z. Zhao, W. Zhang, et al., Adv. Mater. 33 (2021) e2103762.
[85] H. Xu, J. Yuan, G. He, et al., Coord. Chem. Rev. 475 (2023) 214869.
[86] H. Xu, Y. Zhao, Q. Wang, et al., Coord. Chem. Rev. 451 (2022) 214261.
[87] H. Xu, Y. Zhao, G. He, et al., Int. J. Hydrogen Energy 47 (2022) 14257–14279.
[88] H. Xu, C. Wang, G. He, et al., Inorg. Chem. 61 (2022) 14224–14232.
[89] H. Xu, C. Wang, G. He, et al., Dalton Trans. 52 (2023) 8466–8472.
[90] H. Xu, C. Wang, B. Huang, et al., Inorg. Chem. Front. 10 (2023) 2067–2074.
[91] C. Wang, D. Liu, K. Zhang, et al., ACS Appl. Mater. Interfaces 14 (2022) 38669–38676.
[92] D. Liu, H. Xu, C. Wang, et al., J. Mater. Chem. A 9 (2021) 24670–24676.
[93] Q. Niu, M. Yang, D. Luan, et al., Angew. Chem. Int. Ed. 61 (2022) e202213049.
[94] X. Zheng, J. Yang, Z. Xu, et al., Angew. Chem. Int. Ed. 61 (2022) e202205946.
[95] X. Li, K. Zheng, J. Zhang, et al., ACS Omega 7 (2022) 12430–12441.
[96] W. Zheng, M. Liu, L.Y.S. Lee, ACS Catal. 10 (2019) 81–92.
[97] H. Xu, J. Li, X. Chu, Chem. Rec. 23 (2023) e202200244.
[98] S. Zhou, H. Jang, Q. Qin, et al., Angew. Chem. Int. Ed. (2022) e202212196.

[99] Y. Liu, Y. Chen, Y. Tian, et al., Adv. Mater. 34 (2022) e2203615.
[100] J. Li, Y. Tan, M. Zhang, W. Gou, et al., ACS Energy Lett. 7 (2022) 1330–1337.
[101] Y. Tan, Y. Zhu, X. Cao, et al., ACS Catal. 12 (2022) 11821–11829.
[102] H. Xu, J. Li, X. Chu, Nanoscale Horiz. 8 (2023) 441–452.
[103] X. Chu, Y. Liao, L. Wang, et al., Chin. Chem. Lett. 34 (2023) 108285.
[104] M. Yuan, C. Wang, Y. Wang, et al., Nanoscale 13 (2021) 13042–13047.
[105] J. Chen, C. Chen, M. Qin, et al., Nat. Commun. 13 (2022) 5382.
[106] M.J. Hulsey, V. Fung, et al., Angew. Chem. Int. Ed. 61 (2022) e202208237.
[107] X. Kong, J. Xiao, A. Chen, et al., J. Colloid Interface Sci. 608 (2022) 2973–2984.
[108] J. Li, J. Hu, M. Zhang, et al., Nat. Commun. 12 (2021) 3502.
[109] Z.W. Wei, H.J. Wang, C. Zhang, et al., Angew. Chem. Int. Ed. 60 (2021) 16622–16627.
[110] Y. Wang, C. Li, Z. Fan, et al., Nano Lett. 20 (2020) 8074–8080.
[111] Y. Chen, Z. Fan, J. Wang, et al., J. Am. Chem. Soc. 142 (2020) 12760–12766.
[112] N. Zhang, F. Zheng, B. Huang, et al., Adv. Mater. 32 (2020) e1906477.
[113] H. Tao, X. Sun, S. Back, et al., Chem. Sci. 9 (2018) 483–487.
[114] S. Yu, S. Louisia, P. Yang, JACS Au 2 (2022) 562–572.
[115] Y. Yang, S. Louisia, S. Yu, et al., Nature 614 (2023) 262–269.